Soft Matter

PAPER

View Article Online
View Journal | View Issue

Cite this: *Soft Matter*, 2023, **19**, 1606

Preparation of highly stable and ultrasmooth chemically grafted thin films of chitosan†

Cyrielle Garreau,[a] Leonardo Chiappisi,[b] Samantha Micciulla,[b] Isabelle Morfin,[c] Stéphane Trombotto,[a] Thierry Delair[a] and Guillaume Sudre *[a]

Received 2nd January 2023,
Accepted 25th January 2023

DOI: 10.1039/d3sm00003f

rsc.li/soft-matter-journal

Chitosan-coated surfaces are of great interest for biomedical applications (antibacterial coatings, implants, would healing, single-cell microfluidics…). However, one major limitation of chitosan-based systems is the high solubility of the polymer under acidic aqueous conditions. Herein, we describe a simple procedure to prepare extremely smooth and stable chitosan coatings. In detail, chitosan films with a low degree of *N*-acetylation and of thicknesses varying from 40 nm to 10 μm were grafted onto epoxy-functionalized silicon wafers *via* an optimized water–temperature treatment (WTT). The formation of a grafted chitosan network insoluble in acidic aqueous media (pH 3.5) was evidenced and the films were stable for at least 2 days at pH 3.5. The film morphology and the swelling behavior were characterized by atomic force microscopy (AFM) and neutron reflectivity, which showed that the film roughness was extremely low. The physical cross-linking of the films was demonstrated using infrared spectroscopy, dynamic mechanical analysis (DMA) and wide-angle X-ray scattering (WAXS). Finally, we show that the swelling behavior of such films was largely influenced by the environmental conditions, such as the pH or ionic strength of the solution.

1. Introduction

Functionalized surfaces are of great interest due to their wide range of applications in medicine fields, materials, and biology. Indeed, an appropriate polymer coating and especially a stimuli-responsive polymer can provide specific surface properties such as wetting, biocompatibility, adhesion, chemical resistance, or even antibacterial activity. Systems composed of self-assembled layers such as layer-by-layer (LbL) or polymer brushes are widely studied in the literature.[1–3] The use of cross-linked or hydrogel films is another promising solution to obtain a wide range of thicknesses, from nanometers to micrometers.[4–9] Hydrogel films are also able to respond to stimuli such as temperature, pH or ionic strength. In this study, we chose chitosan, a natural polysaccharide produced by biomass.[10] Chitosan is a copolymer made of D-glucosamine (GlcN) and *N*-acetyl-D-glucosamine (GlcNAc) units linked by β (1→4) glycosidic bonds and the molar ratio of acetylated moieties is designated as the degree of *N*-acetylation (DA). Chitosan can be processed in various physical forms, such as gels,[11] nanoparticles,[10] or films,[12] or composite materials.[13] Well-known for its bioactivity, its biocompatibility and its biodegradability, chitosan has been studied in numerous applications including food, cosmetics, agriculture or biomedical fields.[14–18] In recent years for instance, chitosan films have proven particularly useful in bacterial imaging applications,[19,20] opening the way for faster diagnosis methods.[21] However, chitosan coated on surfaces easily dissolves in mild acidic aqueous solutions, due to the protonation of the amine group ($pK_a \sim 6.3$). The solubility of chitosan in acidic media precludes its use for numerous applications such as, for instance, in the biomedical field (antibacterial coatings, implants, would healing, single-cell microfluidics…). Accordingly, numerous attempts to improve the stability of chitosan films have been made. For instance, Park *et al.* showed that the stability of layer-by-layer deposited chitosan carboxymethylcellulose films significantly improved upon chemical cross-linking.[22] However, those multilayer films presented numerous defects after washing with phosphate saline buffer. Other strategies to improve chitosan stability include the use of ionic cross-linkers, such as citric acid or trisphosphate.[23–25]

[a] *Univ Lyon, CNRS, UMR 5223, Ingénierie des Matériaux Polymères, Université Claude Bernard Lyon1, INSA Lyon, Université Jean Monnet, F-69622, Villeurbanne cédex, France. E-mail: guillaume.sudre@univ-lyon1.fr*
[b] *Institut Laue-Langevin, 71 Avenue des Martyrs, Grenoble F-38000, Cedex 9, France*
[c] *LIPhy, Université Grenoble Alpes CNRS, UMR 5588, 140 Avenue de la Physique, Saint Martin d'Hères F-38402, France*

† Electronic supplementary information (ESI) available: Customized cell for neutron reflectivity analysis: silicon blocks clamped against a Teflon trough filled with liquid solution, held by a stainless-steel device. Neutron reflectivity curves of chitosan swollen films and the corresponding fits without including an incoherent sum over areas with small thicknesses. Profiles of scattering length density for chitosan films of a similar thickness (45 nm) immersed in D_2O solutions. See DOI: https://doi.org/10.1039/d3sm00003f

While numerous studies have dealt with crosslinking chitosan chains, to our knowledge, only a few studies about directly grafting chitosan on substrates are reported. Shi *et al.* carried out an *in vitro* study where titanium alloys were functionalized with covalently grafted chitosan or carboxymethyl–chitosan,[26,27] and Wang *et al.* modified medical silicone sheets with carboxymethyl–chitosan.[28] Lee *et al.* succeeded in grafting 6 nm of quaternized chitosan brushes onto silicon surfaces,[29] and Bratskaya *et al.* reported the antibacterial activity of covalently grafted chitosan and chitosan – κ-carrageenan multilayers.[30] Tan *et al.* prepared recyclable materials with sulfated chitosan grafted on silicon wafers.[31]

However, none of these studies controlled the thickness of chitosan or studied its impact on the physicochemical properties of the grafted thin films obtained. Accordingly, in this work, we aimed at preparing chitosan films with variable thickness and high stability even in acidic media. The films were prepared on silicon wafer substrates because they are atomically smooth and transparent to infrared wavelengths and neutrons. Thus, these wafers are totally adapted for multiple characterization techniques such as ellipsometry, contact angle, infrared spectroscopy, neutron reflectivity, *etc.* To fully exploit these characterization techniques, in the perspective of the application of chitosan-thin films in the domain of colorimetric sensors[32] and optical microscopy imaging,[20] the chitosan films should be as smooth as possible. Micrometric-thick films can be useful in the field of microfluidic actuation.[33]

With the view of preparing chitosan thin films for such applications, coatings were prepared by spin-coating or solvent casting followed by hydrothermal treatment. Film thickness was measured by spectroscopic ellipsometry, and surfaces were characterized by atomic force microscopy (AFM) and contact angle. Structural analyses were carried out using attenuated total reflectance infrared spectroscopy (ATR-FTIR) and the crystallinity was determined by Wide-Angle X-ray Scattering (WAXS). Dynamic mechanical analysis (DMA) was also performed on self-supported films to mimic the treatment suffered by chitosan films during the grafting on silicon wafers and thus determine the mechanical properties of such films. Finally, the layer profiles and the swelling behavior of chemically grafted and crosslinked chitosan films were characterized by neutron reflectivity.

2. Materials and methods

2.1. Materials

Chitosan obtained from shrimp shells was provided by Mahtani Chitosan from batch type 244 with a degree of *N*-acetylation (DA) of 0.5% determined by ^{1}H NMR, a mass-average molar mass (M_w) of 196 kg mol^{-1} and a dispersity ($Đ$) of 2.3 determined by size-exclusion chromatography. Acetic acid (AcOH, >99.9% w/w), hydrogen peroxide (H_2O_2, 40% w/w), sulfuric acid (H_2SO_4, 96% w/w), hydrochloric acid (HCl, 37% w/w), ammonium hydroxide (NH_4OH, 28% w/w), toluene, anhydrous toluene, deuterium oxide (99.9% D) and (3-glycidyloxypropyl)trimethoxysilane (GPS, >98%) were purchased from Sigma Aldrich (Merck KGaA, Darmstadt, Germany). Milli-Q water was obtained with an ultrapure water system of type 1 (Simplicity®, resistivity of 18.2 MΩ cm). Silicon wafers (doped-P bore, orientation (100)) were purchased from Siltronix® (Archamps, France) and circular silicon blocks (doped-P bore, orientation (100), D = 5.08 cm, 1 cm thick) were purchased from ACM (Villiers-Saint-Frédéric, France).

2.2. Chitosan preparation

Chitosan was previously filtrated in order to remove insoluble impurities before any use. Chitosan was first solubilized at 0.5% w/v in an AcOH aqueous solution, followed by successive filtrations through cellulose membranes (Millipore®) with decreasing pore sizes from 3 μm to 0.22 μm. Chitosan was then precipitated with NH_4OH and washed several times by centrifugation with Milli-Q water until a neutral pH was obtained. The purified chitosan was finally freeze-dried and stored at room temperature.

2.3. Film preparation

2.3.1. Silanization of silicon substrates. The received wafers were cut into squares measuring approximately 2 × 2 cm^2. In order to clean them from organic pollution and generate the silanol groups at the surface, the silicon substrates were immersed in a piranha bath (H_2SO_4/H_2O_2, 7/3 v/v) heated at 150 °C for 15 min, and then rinsed with Milli-Q water. They were then subjected to ultra-sonication in Milli-Q water for 5 min and dried under a flux of clean air. The modification of freshly cleaned substrates was carried out in a 2% v/v solution of GPS in dry toluene for 5 h as previously described by Sudre *et al.*[34] Silanized wafers were then rinsed with toluene and immersed in an ultra-sonication bath before being dried.

2.3.2. Grafting of chitosan onto silanized substrates. Chitosan was solubilized overnight in an AcOH aqueous solution. The amount of acid added was calculated in stoichiometry compared to amine groups available on chitosan. Chitosan solutions with concentrations ranging from 0.1% to 2% w/v were prepared in this study to deposit various thicknesses on silicon wafers. Chitosan solutions were filtered (0.45 μm) and the films were finally formed onto epoxy-functionalized substrates by spin-coating at 3000 rpm until the solvent evaporates completely (5 min) or by solvent casting. In the case of the solvent casting method, the chitosan solution was poured on the silicon wafer and water was slowly evaporated at room temperature during 24 h to allow the film formation. The epoxy-amine reaction between the epoxy-functionalized wafer and the amine group of the chitosan polymer chain was allowed thanks to a water–temperature treatment (WTT). Practically, coated surfaces were placed in a closed chamber containing a water bath (100% relative humidity) and the container was then placed in an oven at a given temperature and time, the optimization of which will be discussed later. The wafers were then immersed in an acidic solution to remove ungrafted chitosan. The same process was also realized with unfunctionalized wafers to check the efficiency of the grafting and of the acidic washing.

2.4 Physicochemical characterizations of surfaces

2.4.1. Film thickness. Spectroscopic ellipsometry measurements of silanized surfaces were carried out using an ellipsometer (SOPRA GES-5E) at an incident angle of 70°, close to the silicon Brewster angle. Data were then processed using WINELLI (Sopra-SA) software. A Cauchy model was used to fit experimental data ($\cos\Delta$, $\tan\Psi$), in the spectral range of 2.0–4.5 eV, depending on fits and regression qualities, to evaluate the thickness. The UV parameters n and k of the native SiO_2 layer were set respectively to 1.46 and 0.01 while those of the GPS layer were set to 1.429 and 0.01. The thickness of chitosan layers in the dry state was measured using a thin-film analyzer (Filmetrics®, F20-UV model) connected to FILMeasure software. The n and k parameters of chitosan were set respectively to 1.53 and 0.002. For each method, three measurements were done on each film at different positions in order to verify the homogeneity of the film thickness.

2.4.2. Surface topography. The surface morphologies were characterized by atomic force microscopy (AFM) (CSI Nanoobserver) operating in tapping mode. AFM tips with a spring rate close to 3 N m^{-1} were purchased from AppNano. The AFM images were processed using Gwyddion software.

2.4.3. Static contact angles. Contact angles were measured using a tensiometer (Easydrop, Kruss) kit out with a camera connected to a computer equipped with drop shape analysis software. To place the 1 μL liquid drop on the surface, a Hamilton syringe of 1 mL and a needle with a 0.5 mm diameter were used. The contact angle changes over time: it first decreases while the droplet spreads onto the film, and then keeps decreasing while water is evaporated (the triple line does not move anymore). We have chosen to report the contact angle after the drop stops spreading, which corresponds to approximately 10 s after drop deposition.

2.4.4. Fourier transform infrared spectroscopy. FTIR analyses were recorded on a Nicolet iS10 infrared spectrometer operating in attenuated total reflectance Fourier Transform Infrared Spectroscopy mode (ATR-FTIR). A cooled HeCdTe-based detector was used. For chitosan powder analysis, the device was used in the ATR mode with a diamond crystal. The spectra acquisition was performed using 128 scans in a wave number interval ranging from 4000 to 650 cm^{-1} with a resolution of 4 cm^{-1}. For chitosan thin films analysis, a multi-reflection device (Gateway™) purchased from Eurolabo was used with a trapezoidal silicon crystal (specific edge profile cut at 45° angle, with dimensions 70 × 10 × 1 mm). A homemade accessory was added to make the crystal tailored to the device. A wave number interval ranging from 4000 to 1500 cm^{-1} for a resolution of 4 cm^{-1} and a number of 512 scans were selected to perform the experiments.

2.5. Structural characterization of chitosan films

2.5.1. Wide angle X-ray scattering (WAXS) on self-supported films. The wide-angle X-ray scattering patterns of chitosan films were measured at the European Synchrotron Radiation Facility (ESRF, Grenoble, France) on the BM2-D2AM beamline. To prepare the samples, a chitosan solution was poured into Petri dishes and the resulting film of 15 μm thickness was die-cut in a circular shape (D = 12 mm). Chitosan films were then overlaid and stuck with Kapton to obtain a chitosan film thickness of about 150 μm. The scattered patterns of the 150 μm chitosan films were recorded with an incident photon energy of 16 keV, using a two-dimensional photon counting pixel detector placed at 97.4 mm from the sample. The two-dimensional data were corrected by considering the dark images, the detector geometry, and the flat field response of the detector. The signal of the empty cell with Kapton was subtracted from the scattering images of the studied sample. The experiment was performed on films prior and after having been submitted to the WTT.

2.5.2. Dynamic mechanical analysis (DMA) on self-supported films. A chitosan solution was poured into Petri dishes and the resulting film of 14 μm thickness was die-cut in a rectangular shape (15 × 4.5 mm^2). The thermo-mechanical properties of the chitosan thin film were determined in tensile mode using an 850 dynamic mechanical analyzer (TA Instruments) and the humidity was created by a computer-controlled humidifier which produced humid air by mixing dry and fully saturated air streams. The experiments were performed at 70 °C with a relative humidity of 90% and a preload force of 0.2 N, using a deformation amplitude of 5 μm and a frequency of 1 Hz. Data were also recorded during temperature and humidity conditioning. The mechanical properties of the native and annealed films (10 × 4.5 mm^2) of approximatively 20 μm thickness were also evaluated by the tensile test with a constant force rate of 0.1 N min^{-1} and with a preload force of 0.1 N.

2.5.3. Neutron reflectivity. Neutron reflectivity (NR) measurements were carried out on the reflectometer FIGARO at the Institut Laue-Langevin (Grenoble, France).[35] The instrument collimation was set for reflection down mode, with the neutron beam reaching the sample through the silicon substrate at an incident angle of 1°, a wavelength range of 2 Å $< \lambda <$ 20 Å and a full width at half-maximum resolution of about 1%. The settings allow the cover of a momentum transfer vector q range of $0.01 < q/Å^{-1} < 0.043$. The sample surface illuminated by the neutron beam was 35 × 15 mm^2.

Neutron reflectivity experiments were performed at the silicon–water interface using chitosan films and deuterated water. The sample holder is a customized cell which maintains the silicon crystal tightly clamped against a Teflon trough filled with the liquid solution (Fig. S1, ESI†). The liquid solutions used to swell the chitosan films were prepared at different ionic strengths (10 mM and 1000 mM NaCl) and equilibrated at various pH (3.1, 4.6, 5.6 and 8.1) with a minimum amount of NaOH and HCl. As the solutions are prepared with D_2O, these read pH correspond to real pH values of 3.5, 5, 6 and 8.5 according to the equation (pD = pH_{read} + 0.4) of Glasoe and Long.[36]

To analyze the data, the volume fraction profiles normal to the silicon substrate of every component in the system, $\phi_{\{ch\}}(z)$, was modelled. While slabs of given thicknesses and roughness were used to describe the silicon substrate, the silicon oxide layer, and the initiator layer, a continuum description for the chitosan films was opted for. Specifically, the volume fraction

of the chitosan $\phi_{\{ch\}}$ was modelled with an error function, as:

$$\phi_{\{ch\}}(z) = \frac{1}{2}(1-\varphi_h)\mathrm{erfc}\left(\frac{z-d}{\sqrt{2}\sigma_c}\right) \quad (1)$$

with φ_h being the degree of hydration of the chitosan film, d its swollen thickness, and σ_c the film roughness. z is the distance normal to the interface, whereby the choice of fixing $z = 0$ at the initiator/brush layer was taken for convenience. The thickness of the swollen film is linked to the dry polymer amount d_p, given in volume of polymer per surface area, and its degree of hydration φ_h as:

$$d = \frac{d_p}{1-\varphi_h} \quad (2)$$

The scattering length density (SLD) profile, required to compute the neutron reflectivity curve, was obtained as the volume fraction weighted average of the SLDs of the individual components:

$$\mathrm{SLD}(z) = \sum_i \phi_i \mathrm{SLD}_i \quad (3)$$

Finally, the Abeles matrix formalism was used to calculate the corresponding neutron reflectivity curves.[37] To extract physically meaningful parameters, a global least-squares minimization was performed. In particular, all NR data from the same coating were simultaneously fitted, with the dry polymer amount being the shared parameter. The SLD of the dry polymer was fixed and calculated by assuming that the labile hydrogen atoms of alcohol and amine groups were replaced by deuterium atoms since the films were immersed in deuterium oxide solutions. $\mathrm{SLD_{CS}}$ of chitosan was calculated using a specific density of 1.342 g $\mathrm{cm^{-3}}$ and was equal to 3.57×10^{-6} $\mathrm{Å^{-2}}$. The SLD used for silicon, silicon dioxide, GPS and deuterium oxide were respectively equal to $\mathrm{SLD_{Si}} = 2.07 \times 10^{-6}$ $\mathrm{Å^{-2}}$, $\mathrm{SLD_{SiO_2}} = 3.47 \times 10^{-6}$ $\mathrm{Å^{-2}}$, $\mathrm{SLD_{GPS}} = 0.5 \times 10^{-6}$ $\mathrm{Å^{-2}}$ and $\mathrm{SLD_{D_2O}} = 6.23 \times 10^{-6}$ $\mathrm{Å^{-2}}$. In practice, for a set of swelling curves, one global parameter – the chitosan amount – and two individual parameters – the degree of hydration and the film roughness – were optimized.

3. Results and discussion

3.1. Grafting of chitosan thin films on silicon surfaces

3.1.1. Preparation of grafted chitosan coatings with controlled thickness. The first step consisted in forming a silane monolayer by exposing silicon wafers to a 2% v/v GPS solution in toluene. Indeed, silane coupling agents are commonly used to functionalize surfaces for subsequent polymer grafting.[38] The piranha washed wafer presented a contact angle inferior to the experimental resolution of the tensiometer while the silanized one was about 50°–53° which suggests that the surface was indeed modified. A thickness of 1.1 ± 0.1 nm determined by ellipsometry was obtained which is consistent with the literature for monolayers.[34] Chitosan coatings with different thicknesses were obtained either by spin-coating the polymer solution with different concentrations (see Table 1) or by solvent casting. The spin-coating procedure was performed at 2000 rpm during 300 s and led to the formation of thin films up to 300 nm while the solvent casting method allowed much higher thicknesses (~10 μm). The thickness of chitosan films prepared from chitosan solutions at various concentrations was measured by ellipsometry and the results are reported in Table 1.

Table 1 Dry thickness of chitosan films deposited on epoxy-functionalized wafers measured by ellipsometry according to the deposition method and the chitosan concentration

Deposit method	Concentration of chitosan solution used (w/v)	Thickness
Spin-coating	1%	40–60 nm
Spin-coating	2%	150–250 nm
Solvent casting	0.1%	1–2 μm
Solvent casting	1%	10–12 μm

3.1.2. Influence of the reaction time and the temperature. In order to optimize the grafting, water–temperature treatments were carried out at various temperatures and times on chitosan films prepared from a 1% w/v solution spin-coated on silicon wafers. A saturated humidity was introduced to make the chitosan swell and improve the chitosan chain mobility. The heating allowed the reaction between the amino group of chitosan chain and the epoxy group of the silanized silicon wafers (Scheme 1).

Once the water–temperature treatment was carried out by exposing the coated surfaces to high temperatures for different times, the surfaces were immersed in an acidic aqueous solution (AcOH) at pH 3.5 for 2 days to solubilize and therefore remove ungrafted chitosan. Chitosan film thicknesses were measured by ellipsometry at different steps of the process, for which temperature and time were varied (see Fig. 1). The initial thicknesses of the films (in dark red and dark blue) may slightly vary due to silicon modification, and small variations in chitosan solution concentration and relative humidity during spin-coating.

The experiments were also realized with unfunctionalized wafers to check the efficiency of the grafting and of the acidic washing. As we can see in Fig. 1 (red bars), chitosan spin-coated on native wafers was removed irrespective of the WTT conditions. This result means that the acidic washing is effective to remove ungrafted chitosan. The residual chitosan layer on these substrates, a few nanometers thick only, can originate from the strong adsorption of a small amount of chitosan. Fig. 1 also shows that a heating treatment performed at 50 °C for 48 h or at 70 °C for 15 h was not sufficient to obtain a stable coating (blue bars). The acidic aqueous washing removed most of the chitosan coating and led to the formation of heterogeneous coatings. When the reaction was performed at 70 °C and for a longer reaction time (24 h or 72 h), the overall chitosan thickness was not reduced despite the acidic aqueous washing in AcOH at pH 3.5 as a result of the chemical grafting of chitosan onto the surfaces. Additionally, these surfaces remained stable in a neutral aqueous environment for 7 days and in strong acidic aqueous medium (HCl, pH 2.5)

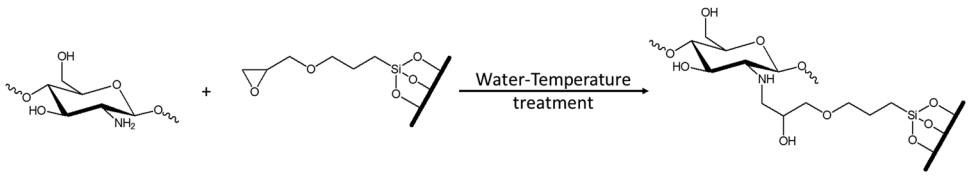

Scheme 1 Schematic representation of the chemical reaction occurring at the interface between some glucosamine moieties and the epoxy-functionalized wafer.

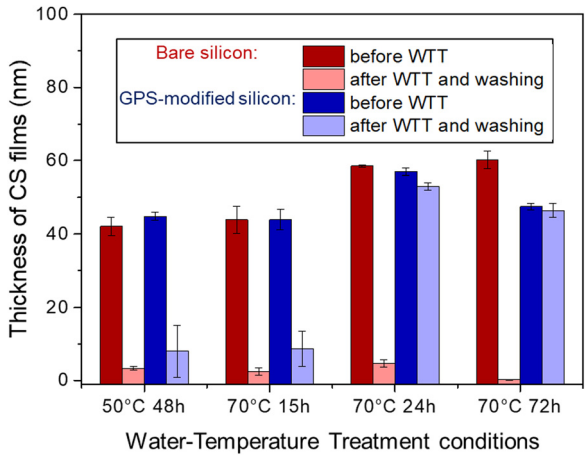

Fig. 1 Thickness variation upon water–temperature treatments (WTT) and unbound chitosan (CS) removal by acidic aqueous washing: thickness of chitosan films on unfunctionalized wafers (dark red) before WTT (*i.e.* after spin-coating) and (light red) after WTT and 2 day acidic aqueous washing (AcOH, pH 3.5). Thickness of chitosan films on epoxy-functionalized wafers (dark blue) before WTT (*i.e.* after spin-coating) and (light blue) after WTT and 2 day acidic aqueous washing (AcOH, pH 3.5).

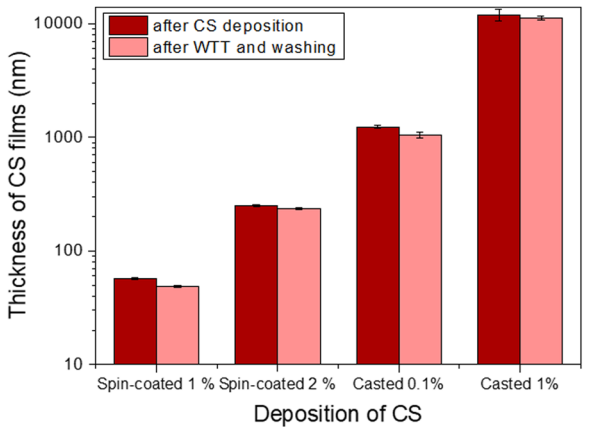

Fig. 2 Thickness of chitosan (CS) films on epoxy-functionalized wafers (dark red) before water–temperature treatment (WTT) (*i.e.* after spin-coating or solvent casting of chitosan solutions at various concentrations % m/v) and (light red) after WTT and 2 day acidic aqueous washing (AcOH, pH 3.5).

for 2 days. However, unlike chitosan films annealed during 24 h, the ones processed for 72 h were slightly yellow: given the long exposition at 70 °C, side reactions – such as Maillard reaction[39] or caramelization – may occur, responsible for the weak color change of the film.[40] Hence, for further characterizations, we selected only films grafted at 70 °C for 24 h. In summary, the water–temperature treatment of spin-coated films on epoxy-functionalized wafers allows us to prepare stable chitosan films with a simple, scalable, and low-cost procedure.

3.1.3. Influence of the thickness of the film. The efficacy of the WTT, optimized above (70 °C, 24 h, 100% RH), was assayed as a function of the thickness of chitosan films (from about 40 nm to 11 μm). Surfaces were washed in an acidic aqueous solution (AcOH, pH 3.5) for 2 days and the remaining thicknesses were measured by ellipsometry. The results are presented in Fig. 2. Chitosan films up to 11 μm were homogeneously grafted on the substrates, though a very slight decrease in thickness (evaluated between 5 and 15%) was observed after the WTT and the acidic aqueous washing. This might be attributed to film shrinking caused by the annealing, as previously described in the literature. Indeed, Murray and Dutcher showed that a thermal treatment could reduce significantly the film thickness and they assigned this observation to the desorption of the water trapped in the polymer matrix.[41] The small loss of material upon acidic aqueous washing also indicates that chemical physical cross-linking occurs between the chitosan chains within the film, and not only between the polysaccharide and the substrate. Further deep physicochemical characterizations were carried out to shed light on the side phenomena which may lead to the apparent cross-linking of the film.

3.2. Surface characterization of chitosan grafted films

3.2.1. Surface topography. The morphology of the chemically grafted films was characterized by carrying out AFM imaging on films of various thicknesses (Fig. 3). AFM images were recorded over an area of 10 μm × 10 μm and the roughnesses were measured by the root-mean-square deviation of the surface (RMS).

All the prepared films were very smooth, with an RMS roughness lower than 2 nm for the thin spin-coated films and less than 5 nm for the thicker film prepared by solvent casting. A similar roughness was observed with the adsorbed thin films prepared in the same way by Diallo, meaning there is no impact of the heating treatment on the surface morphology.[42] However, some differences can be noticed when varying the thickness.

3.2.2. Water wetting properties. To investigate the wettability of the modified surfaces, water contact angles were

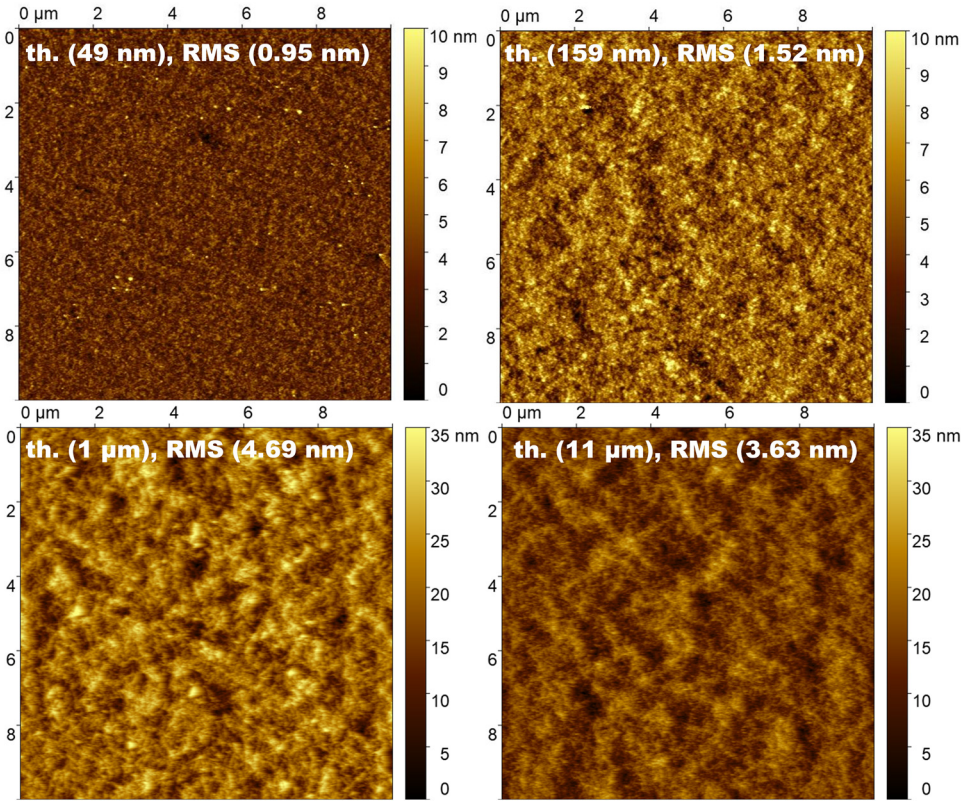

Fig. 3 AFM images of chitosan grafted films (DA 0%) with various thicknesses and the corresponding RMS roughness. Please note the different height-scale for the different images.

Table 2 Water contact angle measurements of chitosan grafted films for various film thicknesses

Thickness	Water contact angle (°)
60 nm	78.8 ± 1.0
235 nm	79.5 ± 0.7
1 μm	76.2 ± 1.7
11 μm	79.4 ± 2.5

measured 72 h after the grafting. The analysis was delicate as chitosan chains present on the surfaces quickly interact with water molecules. An equilibration time of 10 seconds was chosen after the drop deposition to allow for chitosan swelling without dealing with drop evaporation. Contact angles of chitosan grafted films for various thicknesses are shown in Table 2.

All the surfaces presented a high contact angle ranging from 76.2° to 79.5° which can be easily explained by the low affinity of deacetylated chitosan with water when the chitosan film obtained is in the neutral state. These results are consistent with previous studies which have shown the NH_3^+ groups of chitosan coating are neutralized when prepared from AcOH solutions.[42,43]

3.3. Structural analysis of chitosan grafted films

3.3.1. Chemical structure of chitosan grafted films. Structural analysis of chitosan grafted films was carried out using ATR-FTIR spectroscopy on silicon crystals. The influence of each step of the preparation process on the chitosan structure was investigated. Thus, IR spectra were obtained after the spin-coating of chitosan solution, after the water temperature treatment (70 °C, 24 h, 100% RH) and after the 2 day acidic aqueous washing in AcOH at pH 3.5. In order to understand the chitosan structure when the polymer is thin film shaped and processed, analyses were also carried out for the native chitosan powder by ATR-FTIR spectroscopy. The spectra are presented in Fig. 4. Each spectrum shows the expected absorption band for chitosan at 1585 cm^{-1} corresponding to the bending vibration of the primary amino group $–NH_2$. The $–NH_2$ absorption band of the spin-coated chitosan slightly shifts to 1560 cm^{-1} due to the cationic state of the chitosan film (Fig. 4b) shortly after spin-coating, when chitosan remains under the chitosan acetate form and the amino group is protonated ($–NH_3^+$). The small bump observed around 1655 cm^{-1} can be attributed to the stretching vibration of C═O of the acetylated units. Most notably, the water–temperature treatment affects the broad vibration band centered at 3300 cm^{-1}, that corresponds to the contribution of inter- and intramolecular hydrogen bonds of –NH and –OH groups. In particular, three sharp peaks are visible after WTT in the region 3400–3500 cm^{-1}. These distinct peaks suggest that the type of hydrogen bonds in the films is modified with annealing, *i.e.*, the characteristic distances between the same atoms of the same molecules are modified. The sharpness of the peaks further indicates an increase in

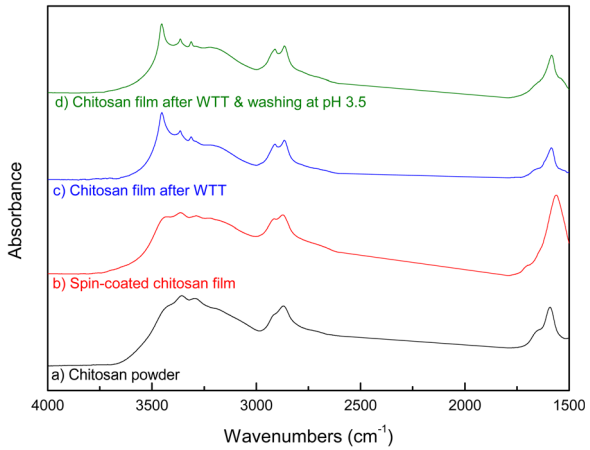

Fig. 4 ATR-FTIR spectra of chitosan grafted films at various steps of the process. (a) Chitosan starting powder, (b) chitosan film after spin-coating on silicon crystal, (c) chitosan film after the water–temperature treatment (WTT, 70 °C, 24 h, 100% RH), and (d) chitosan film after washing in acidic aqueous media (AcOH, pH 3.5). Spectra are normalized relative to the C–H stretching bond at 2900 cm^{-1}. Curves were vertically shifted for clarity.

crystallinity and loss of water, associated to a reduced solubility of such films in aqueous media.[44–47]

3.3.2. Mechanical properties of self-supported chitosan films. DMA measurements were carried out to evaluate the effect of the WTT on the mechanical properties of the chitosan films and to understand why the film cannot be dissolved after heating. More precisely, the aim of the experiment was to mimic the annealing of chitosan films performed in a humidity environment to graft them on silicon wafers. To do that, the self-supported films were placed in the DMA chamber. The temperature and relative humidity (RH) were set respectively to 70 °C and 90% and the storage modulus was recorded during the two conditioning steps as illustrated respectively in Fig. 5(A)a and b. Then, Fig. 5(A)c shows the evolution of the storage modulus of a chitosan film annealed for 24 h at 70 °C with 90% RH. Finally, the humidity and the temperature were respectively set to 0% and 30 °C (Fig. 5(A)d and e).

A storage modulus of 4.0 GPa was determined for the chitosan film initially placed at 70 °C. Then, the film showed a meaningful decrease of the storage modulus while the relative humidity was increased. It can be explained by the uptake of water, which acts as a plasticizer and allows chitosan to swell. These observations are consistent with the behavior described by Fernandes *et al.*[48] and Micciulla *et al.*[49] Then, when heated at 70 °C for 24 h with a RH of 90%, the storage modulus of the film increased from 0.17 GPa to 0.33 GPa. Additionally, the tensile test experiments with a ramp force revealed that the native chitosan film showed a strain at break around 31% while the annealed film presented a strain at break around 12% (Fig. 5(B)). Some studies explained this behavior by the crystallinity of the chitosan films.[50–52] Indeed, crystalline regions will increase the fragility of the films and lead to a lower strain at break. Foster *et al.* also showed that an uptake of water in chitosan films resulted in a lower tensile strength but a higher strain at break.[53] This reinforces the hypothesis that desorption of water occurred with the annealing: the results from DMA suggest that 90% RH is enough to obtain a WTT that modifies the structure of the film. This decrease in water content could result in physical crosslinking and could explain the increase in storage modulus obtained when a chitosan film was heated at 70 °C for 24 h. These observations are consistent with the previous ATR-FTIR experiments which showed a change in the hydrogen bonding and, thus, which might suggest a change in crystallinity.

3.3.3. Crystalline structure of self-supported chitosan films. Wide Angle X-ray Scattering was performed on self-supported films to evaluate the effect of the WTT on their crystalline structure. Fig. 6 shows the diffraction diagram of a self-supported chitosan film dried at room temperature for a few days and the same film after performing a WTT at 70 °C for 24 h at 100% RH. Before annealing, a similar diffractogram was obtained by Becerra *et al.* for a non-neutralized chitosan film

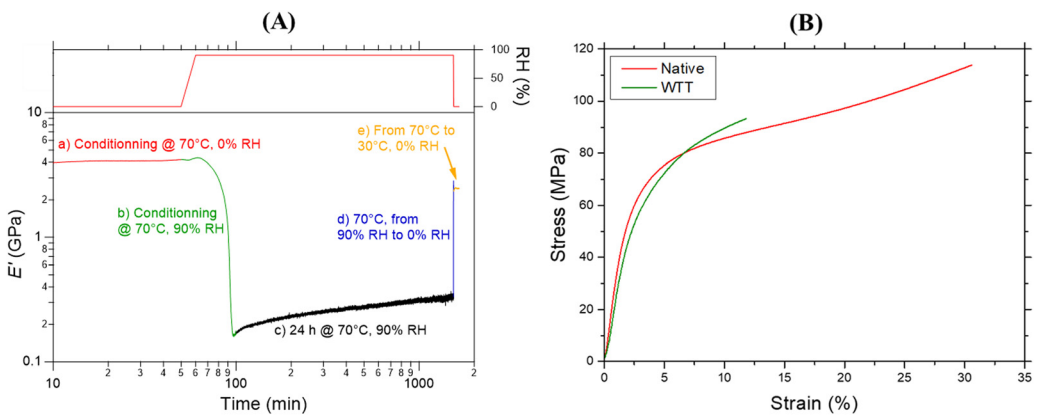

Fig. 5 DMA curves of self-supported chitosan thin films: (A) evolution of the storage modulus at various step of the process (a) temperature conditioning (70 °C), (b) humidity conditioning (90% RH), (c) time sweep (24 h, 70 °C, 90% RH), (d) humidity decreasing (0% RH) and (e) temperature decreasing (30 °C). The RH variation is plotted as a function of time on the right axis. (B) Stress-strain curves of native (dry at RT during few days) and after the water–temperature treatment (WTT, 70 °C, 24 h, 100% RH) chitosan films. The (B) experiment was performed at ambient humidity.

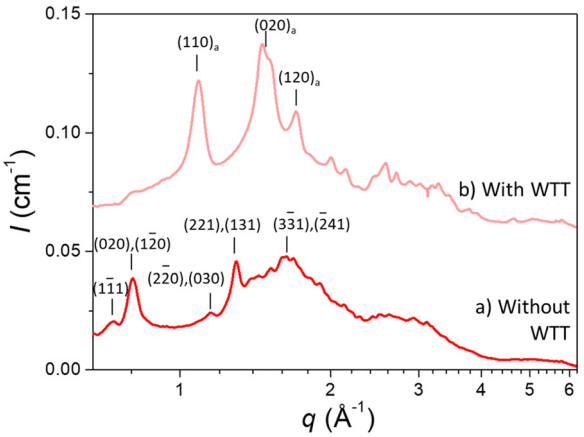

Fig. 6 Diffraction diagrams of (a) a self-supported chitosan film dried at room temperature for a few days and (b) the same film after water–temperature treatment at 70 °C for 24 h at 100% RH. For the sake of clarity, curve b was vertically shifted (I + 0.05).

dried at room temperature over a week.[54] It is characteristic of the chitosan acetate salt. Indeed, chitosan films present different crystalline structures depending on the preparation method and more specifically on the neutralization state of the film.[43,55] The anhydrous allomorph is then observed after the WTT with reflections around q = 1.09 Å^{-1}, q = 1.46 Å^{-1} and q = 1.70 Å^{-1} as shown in Fig. 6b. These peaks are respectively characteristics of the $(110)_a$, $(020)_a$ and $(120)_a$ reflections of the anhydrous allomorph.[54]

Thus, the crystallinity of the low DA chitosan shifts from the crystalline acetate salt to the anhydrous allomorph. As a consequence, water is no longer involved in the crystalline structure and the acetic acid has desorbed from the chitosan film. Ogawa has already observed in several studies the removal of water molecules in the unit cell when low DA chitosan was heated, either when a chitosan powder was suspended in water[56] or when a chitosan film was immersed in water after neutralization in NaOH solution.[57] Becerra *et al.* also obtained an anhydrous allomorph of chitosan after a neutralization step in ammonia vapors[54] and Okuyama *et al.* by keeping a chitosan/acetic acid complex in 100% RH at room temperature for several days or with annealing in water.[58] Thus, the crystalline structure of the chitosan films depends both on the annealing and protonation state of chitosan. In our study, acetic acid evaporated during the WTT (see Fig. 4b and c) allowing the film neutralization. Moreover, the peak intensities of the native film (Fig. 6a) are weaker than those of the heated one (Fig. 6b) suggesting an increase of the index of crystallinity after annealing. These observations corroborate the study of Balau *et al.* which indicates that the index of crystallinity is improved with a heating treatment.[59] Our results are also consistent with the modification of hydrogen bonds and with the increase of the storage modulus previously observed which suggested an increase in the chain organization and thus in the crystallinity. Moreover, when the crystallization state of chitosan is high and in an anhydrous allomorph, chitosan cannot be dissolved in the usual acidic aqueous media, as observed with our films even with a thickness up to 11 μm. Indeed, this decrease of aqueous solubility has been reported many times after heating treatment.[45,46] The higher the annealing temperature or time, the lower the solubility.[46,60]

3.3.4. Swelling behavior and layer profiles of chitosan grafted films. Neutron reflectivity (NR) was used to determine the density profiles and the swelling behavior of the chitosan grafted films when immersed in an aqueous solution. The NR is sensitive to the scattering length density SLD(z) profile in the direction normal to the interface and consequently to the profile of the volume fraction of chitosan.

Each swelling series was fitted globally, using one common value for the chitosan amount in the coating, and for each pH or salinity condition the water content of the film was fitted. To improve the quality of the fit, an incoherent sum over areas with slightly different thickness was included in the fitting routine (see fits without including an incoherent sum in Fig. S2 of the ESI†). In practice, the calculated NR curve was obtained as the integral of polymer dry thickness normally distributed around the average d_p, as:

$$RR(q, d_p, \sigma_c, \sigma_{inc}) = \int \frac{1}{\sigma_{inc}\sqrt{2\pi}} \exp\left[-\frac{1}{2}\left(\frac{x - d_p}{\sigma_{inc}}\right)^2\right] RR(q, x, \sigma_c)\mathrm{d}x \quad (4)$$

In summary, each swelling series is characterized by an average chitosan amount, and for each pH and ionic strength condition, a degree of hydration φ_h, a local roughness σ_c, and a long-range inhomogeneity of the film thickness σ_{inc} are obtained. The choice of two roughnesses is rather uncommon and is motivated by the fact that the films are extremely smooth. In practice, the local roughness has an effect on the depth of the oscillation and on the overall reflected intensity, with $RR(q)$ decaying faster with q for rougher films. Adding a long-range roughness, *i.e.*, different regions on the substrate having on average a different thickness, allows the depth of the minima to be reduced without affecting the reflected intensity.

Fig. 7(a) shows the NR curves and the volume fraction profile of chitosan normal to the silicon substrate corresponding to the best fit of the data for the same chitosan film (45 nm, DA 0%) immersed in a D_2O solution (with 10 mM NaCl) at decreasing pH (8.5, 6.0, 5.0 and 3.5). The corresponding profiles of scattering length density are shown in Fig. S3 (ESI†). The degree of hydration φ_h of the films and their local roughness are reported in Table 3. The coatings were extremely smooth, with roughness values mostly below 0.1% (see Table 3 for values). In combination with the excellent instrumental resolution, up to 7 oscillations were found in the NR data. This is a very uncommon finding in soft matter systems. Indeed, for instance, Li *et al.* obtained much fewer oscillations for chemical networks.[4] This surprisingly high number of Kiessig fringes indicates that the density profiles of our chitosan layers are extremely sharp.

The water content of the hydrated film increases when the pH decreases which is an indication of the increase of the swelling the film. Indeed, the higher the fraction of water,

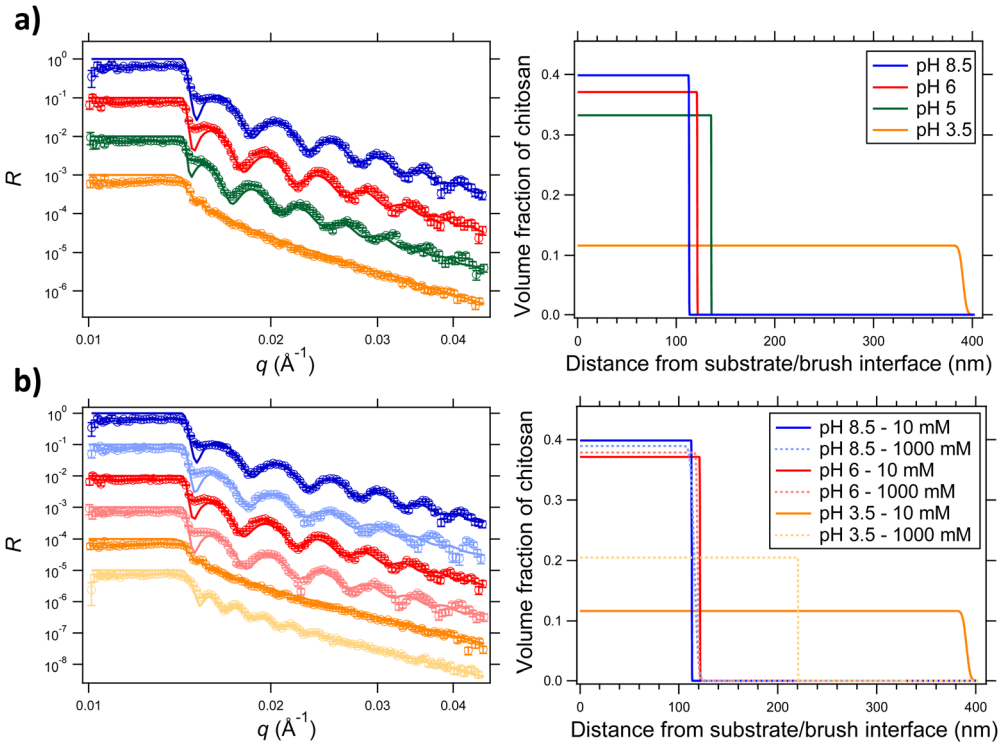

Fig. 7 Neutron reflectivity curves and volume fraction profiles of chitosan normal to the silicon substrate for chitosan films of similar thickness (45 nm) immersed (a) in a D_2O solution (with 10 mM NaCl) at different pH: 8.5, 6.0, 5.0 and 3.5 or (b) in a D_2O solution (pH 8.5, 6.0 and 3.5) at various ionic strengths: 10 and 1000 mM NaCl.

Table 3 Fitted values of the degree of hydration φ_h, the roughness and the swollen thickness for chitosan films of similar dry thickness (45 nm) immersed in a D_2O solution (with 10 mM or 1000 mM NaCl) at different pH: 8.5, 6.0, 5.0 and 35

pH	Ionic strength (mM NaCl)	Degree of hydration φ_h	Swollen thickness (nm)	Local roughness (nm)
8.5	10	0.60	113.1	0.2
6.0	10	0.63	121.4	0.2
5.0	10	0.67	135.7	0.1
3.5	10	0.88	390.7	3.0
8.5	1000	0.61	115.8	3.0
6.0	1000	0.62	119.1	1.0
3.5	1000	0.80	220.5	0.1

the higher the swelling, the closer the SLD from that of the immersing solution (mainly D_2O in our case: 6.23×10^{-6} Å^{-2}) and the lower the volume fraction of chitosan inside the film. Thus, the thickness of the hydrated films deduced from the fitting increases with decreasing pH. Those results can be explained by the osmotic pressure and the charge density of DA 0% chitosan film. The osmotic pressure, which drives the swelling, increases when the pH decreases because of the increasing charge density within the film. When the chitosan film was immersed in a solution at a pH lower than 6.3, the amino groups of the glucosamine units are mostly protonated. Usually, the immersion in acidic medium results in the dissolution of the films[61] and thus the impossibility of performing the NR analysis below pH 5.5.[42] However, the heating treatment performed on our chitosan films increased the crystallinity and shifted it to an anhydrous form that affected the solubility of the films in aqueous solutions and thus their swelling properties. At very low pH, the osmotic pressure becomes higher due to the significant charge density within the film below the pK_a. As a result, the swelling capacity of the chitosan film increased, though without solubilization.

The impact of the ionic strength was also investigated. Fig. 7(b) represents the NR curves and the volume fraction profiles of chitosan normal to the silicon substrate for the same chitosan film (45 nm, DA 0%) immersed in a D_2O solution with increasing ionic strength. At pH 3.5, the water content (Table 3) and thus the swollen thickness clearly decreased when the ionic strength increased from 10 to 1000 mM NaCl. This thickness decrease was due to an increase in the charge screening effect when the ionic strength of the medium increased. Moreover, the higher the charge density on chitosan (at low pH) the more marked the decrease in thickness. Indeed, at higher pH (6.0 and 8.5), the impact of the ionic strength was less pronounced due to the lower charge density of the film. As a consequence, approximately similar water content and volume fraction of chitosan were found, and thus the swellings observed were similar at high pH when varying the ionic strength.

4. Conclusion

Ultra-smooth and stable chitosan films, with thickness ranging from a few tens of nanometers to several micrometers were successfully grafted onto epoxy-functionalized silicon wafers.

This procedure is simple and easily scalable. In particular, chitosan films with an overall thickness up to a few hundreds of nanometers can be prepared by spin-coating, while coatings with an overall thickness of 1–10 micrometers were prepared by solvent casting. The deposition was followed by a water–temperature treatment, under optimal conditions to achieve homogeneously grafted chitosan films at 70 °C and 100%RH for 24 h. The hydrothermal treatment not only promoted the covalent grafting of the chitosan chain to the epoxy-functionalized substrate, but also triggered crystallization within the film, which acts as a physical crosslink. These modifications make it possible to prepare films which are stable in acidic aqueous media (AcOH, pH 3.5) for at least 2 days (for a few seconds without covalent grafting) and in neutral environments for 7 days. Moreover, the film homogeneously swells in water, and the degree of swelling is controlled by the pH and ionic strength of the solution.

We anticipate that the procedure presented in this work is of high interest for practical applications. On the one hand, the procedure allows preparing long-term stable chitosan coatings, also in an acidic environment, thus overcoming one of the main limitations of chitosan. This easy and fast grafting process could be extended to other substrates such as metals or silicones. Moreover, chitosan films prepared with a controlled thickness and impressively low roughness – less than 0.05% for the 11 micrometer thick film with a roughness of less than 5 nm – open up the way for systematic studies on the interaction of chitosan films with pathogens, proteins, or lipid bilayers with ultra-sensitive techniques, such as neutron, light or X-ray reflectometry,[62,63] quartz-crystal microbalance,[64,65] or evanescent wave spectroscopy.[66,67]

Author contributions

This manuscript was written through contributions of all authors. All authors have given approval to the final version of the manuscript.

Abbreviations

AcOH	Acetic acid
AFM	Atomic force microscope
DA	Degree of *N*-acetylation
DMA	Dynamic mechanical analysis
WTT	Water–temperature treatment
GPS	(3-Glycidyloxypropyl)trimethoxysilane
NR	Neutron reflectivity
RH	Relative humidity
RMS	Root mean square
WAXS	Wide angle X-ray scattering

Conflicts of interest

The authors declare no competing financial interest.

Acknowledgements

This study was funded by the French Ministry of Higher Education, Research and Innovation. The authors thank the Institut Laue-Langevin for giving us access to the neutron reflectometer FIGARO (data available at DOI: **10.5291/ILL-DATA.9-11-1982**), the Partnership for Soft Condensed Matter (PSCM) for access to support laboratories, and Philipp Gutfreund for his advices during the experiment and data analysis. We also thank the European Synchrotron Radiation Facility (ESRF, Grenoble, France) for the WAXS measurements on the BM2-D2AM beamline. The Wide-angle X-ray detector (WOS) was funded by the French National Research Agency (ANR) under the ''Investissement d'Avenir'' program (Grant no. ANR-11-EQPX-0010).

References

1 D. Alkekhia and A. Shukla, *J. Biomed. Mater. Res., Part A*, 2019, **107**, 1324–1339.
2 S. Yan, L. Song, S. Luan, Z. Xin, S. Du, H. Shi, S. Yuan, Y. Yang and J. Yin, *Colloids Surf., B*, 2017, **150**, 250–260.
3 I. Luzinov, S. Minko and V. V. Tsukruk, *Prog. Polym. Sci.*, 2004, **29**, 635–698.
4 M. Li, B. Bresson, F. Cousin, C. Fretigny and Y. Tran, *Langmuir*, 2015, **31**, 11516–11524.
5 E. Martwong and Y. Tran, *Langmuir*, 2021, **37**, 8585–8593.
6 M. He, Q. Wang, R. Wang, Y. Xie, W. Zhao and C. Zhao, *ACS Appl. Mater. Interfaces*, 2017, **9**, 15962–15974.
7 B. Chollet, M. Li, E. Martwong, B. Bresson, C. Fretigny, P. Tabeling and Y. Tran, *ACS Appl. Mater. Interfaces*, 2016, **8**, 11729–11738.
8 F. Seidi, W. Zhao, H. Xiao, Y. Jin, M. R. Saeb and C. Zhao, *Polym. Chem.*, 2020, **11**, 4355–4381.
9 F. Paquin, J. Rivnay, A. Salleo, N. Stingelin and C. Silva, *J. Mater. Chem. C*, 2015, **3**, 10715–10722.
10 D. Elieh-Ali-Komi and M. R. Hamblin, *Int. J. Adv. Res.*, 2016, **4**, 411–427.
11 N. Bhattarai, J. Gunn and M. Zhang, *Adv. Drug Delivery Rev.*, 2010, **62**, 83–99.
12 F. S. Ligler, B. M. Lingerfelt, R. P. Price and P. E. Schoen, *Langmuir*, 2001, **17**, 5082–5084.
13 G. Cavallaro, S. Micciulla, L. Chiappisi and G. Lazzara, *J. Mater. Chem. B*, 2021, **9**, 594–611.
14 N. Morin-Crini, E. Lichtfouse, G. Torri and G. Crini, *Environ. Chem. Lett.*, 2019, **17**, 1667–1692.
15 I. Hamed, F. Özogul and J. M. Regenstein, *Trends Food Sci. Technol.*, 2016, **48**, 40–50.
16 W. Xia, P. Liu, J. Zhang and J. Chen, *Food Hydrocolloids*, 2011, **25**, 170–179.
17 M. Dash, F. Chiellini, R. M. Ottenbrite and E. Chiellini, *Prog. Polym. Sci.*, 2011, **36**, 981–1014.
18 W. Wang, C. Xue and X. Mao, *Int. J. Biol. Macromol.*, 2020, **164**, 4532–4546.
19 A. H. Delcour, A. Ducret, O. Théodoly and T. Mignot, *Bact. Cell Surf.*, 2013, **966**, 97–107.

20 J. Tréguier, L. Bugnicourt, G. Gay, M. Diallo, S. T. Islam, A. Toro, L. David, O. Théodoly, G. Sudre and T. Mignot, *mBio*, 2019, **10**(4), e01375-19, DOI: 10.1128/mBio.01375-19.
21 T. Mignot, O. Theodoly-Lannes, G. Sudre, L. David, L. Bugnicourt-Moreira and J. Treguier, WO2019229198A1, 2019.
22 S. Park, J. Park, J. Heo, S. E. Lee, J. W. Shin, M. Chang and J. Hong, *J. Ind. Eng. Chem.*, 2018, **68**, 229–237.
23 G. Infurna, G. Cavallaro, G. Lazzara, S. Milioto and N. T. Dintcheva, *Molecules*, 2021, **26**(11), 3548, DOI: 10.3390/molecules26113468.
24 L. Wen, Y. Liang, Z. Lin, D. Xie, Z. Zheng, C. Xu and B. Lin, *Polymer*, 2021, **230**, 124048.
25 F. Han Lyn, C. P. Tan, R. M. Zawawi and Z. A. Nur Hanani, *J. Appl. Polym. Sci.*, 2021, **138**, 50618.
26 Z. Shi, K. G. Neoh, E. T. Kang, C. Poh and W. Wang, *J. Biomed. Mater. Res., Part A*, 2008, **86**, 865–872.
27 Z. Shi, K. G. Neoh, E. T. Kang, K. P. Chye and W. Wang, *Biomacromolecules*, 2009, **10**, 1603–1611.
28 R. Wang, K. G. Neoh, Z. Shi, E. T. Kang, P. A. Tambyah and E. Chiong, *Biotechnol. Bioeng.*, 2012, **109**, 336–345.
29 H. S. Lee, D. M. Eckmann, D. Lee, N. J. Hickok and R. J. Composto, *Langmuir*, 2011, **27**, 12458–12465.
30 S. Bratskaya, D. Marinin, F. Simon, A. Synytska, S. Zschoche, H. J. Busscher, D. Jager and H. C. van der Mei, *Biomacromolecules*, 2007, **8**, 2960–2968.
31 M. Tan, H. Wang, Y. Wang, G. Chen, L. Yuan and H. Chen, *J. Mater. Chem. B*, 2014, **2**, 569–576.
32 D. Kesal, S. Christau, M. Trapp, P. Krause and R. von Klitzing, *Phys. Chem. Chem. Phys.*, 2017, **19**, 30636–30646.
33 C. Vergne, F. Monti, P. Tabeling, Y. Tran and L. Devys, *Bull. Am. Phys. Soc.*, 2012, **57**(1), W50.11, http://meetings.aps.org/link/BAPS.2012.MAR.W50.11.
34 G. Sudre, E. Siband, D. Hourdet, C. Creton, F. Cousin and Y. Tran, *Macromol. Chem. Phys.*, 2012, **213**, 293–300.
35 R. A. Campbell, H. P. Wacklin, I. Sutton, R. Cubitt and G. Fragneto, *Eur. Phys. J. Plus*, 2011, **126**, 1–22.
36 P. K. Glasoe and F. A. Long, *J. Phys. Chem.*, 1960, **64**, 188–190.
37 F. Abelès, *J. Phys. Radium*, 1950, **11**, 307–309.
38 C. Haensch, S. Hoeppener and U. S. Schubert, *Chem. Soc. Rev.*, 2010, **39**, 2323–2334.
39 I. Leceta, P. Guerrero, I. Ibarburu, M. T. Dueñas and K. de la Caba, *J. Food Eng.*, 2013, **116**, 889–899.
40 M. Villamiel, M. D. del Castillo and N. Corzo, *Food Biochemistry and Food Processing*, John Wiley & Sons, Ltd, 2006, pp. 71–100.
41 C. A. Murray and J. R. Dutcher, *Biomacromolecules*, 2006, **7**, 3460–3465.
42 M. Diallo, *Préparation et caractérisations physicochimiques et biologiques de surfaces modifiées par du chitosane*, PhD thesis, Université de Lyon, 2018.
43 S. Demarger-Andre and A. Domard, *Carbohydr. Polym.*, 1994, **23**, 211–219.
44 S. Rivero, M. A. García and A. Pinotti, *J. Agric. Food Chem.*, 2012, **60**, 492–499.
45 L. Y. Lim, E. Khor and C. E. Ling, *J. Biomed. Mater. Res.*, 1999, **48**, 111–116.
46 L. Y. Lim and L. S. C. Wan, *Drug Dev. Ind. Pharm.*, 1995, **21**, 839–846.
47 I. Leceta, P. Guerrero, I. Ibarburu, M. T. Dueñas and K. De La Caba, *J. Food Eng.*, 2013, **116**, 889–899.
48 S. C. M. Fernandes, C. S. R. Freire, A. J. D. Silvestre, C. Pascoal Neto, A. Gandini, L. A. Berglund and L. Salmén, *Carbohydr. Polym.*, 2010, **81**, 394–401.
49 S. Micciulla, D. W. Hayward, Y. Gerelli, A. Panzarella, R. von Klitzing, M. Gradzielski and L. Chiappisi, *Commun. Chem.*, 2019, **2**, 61, DOI: 10.1038/s42004-019-0155-y.
50 C. Wenling, J. Duohui, L. Jiamou, G. Yandao, Z. Nanming and Z. Xiufang, *J. Biomater. Appl.*, 2005, **20**, 157–177.
51 Y. Wan, K. A. M. Creber, B. Peppley and V. T. Bui, *Polymer*, 2003, **44**, 1057–1065.
52 K. Tomihata and Y. Ikada, *Biomaterials*, 1997, **18**, 567–575.
53 L. J. R. Foster, S. Ho, J. Hook, M. Basuki and H. Marçal, *PLoS One*, 2015, **10**, 1–22.
54 J. Becerra, G. Sudre, I. Royaud, R. Montserret, B. Verrier, C. Rochas, T. Delair and L. David, *AAPS PharmSciTech*, 2017, **18**, 1070–1083.
55 K. Ogawa, T. Yui and M. Miya, *Biosci., Biotechnol., Biochem.*, 1992, **56**, 858–862.
56 K. Ogawa, *Agric. Biol. Chem.*, 1991, **55**, 2375–2379.
57 K. Ogawa, S. Hirano, T. Miyanishi, T. Yui and T. Watanabe, *Macromolecules*, 1984, **17**, 973–975.
58 K. Okuyama, K. Noguchi, M. Kanenari, T. Egawa, K. Osawa and K. Ogawa, *Carbohydr. Polym.*, 2000, **41**, 237–247.
59 L. Balau, G. Lisa, M. I. Popa, V. Tura and V. Melnig, *Cent. Eur. Sci. Journals*, 2004, **2**, 638–647.
60 G. C. Ritthidej, T. Phaechamud and T. Koizumi, *Int. J. Pharm.*, 2002, **232**, 11–22.
61 J. Nunthanid, S. Puttipipatkhachorn, K. Yamamoto and G. E. Peck, *Drug Dev. Ind. Pharm.*, 2001, **27**, 143–157.
62 M. W. A. Skoda, *Curr. Opin. Colloid Interface Sci.*, 2019, **42**, 41–54.
63 C. L. Schauer, M.-S. Chen, R. R. Price, P. E. Schoen and F. S. Ligler, *Environ. Sci. Technol.*, 2004, **38**, 4409–4413.
64 S. Zhang, H. Bai, J. Luo, P. Yang and J. Cai, *Analyst*, 2014, **139**, 6259–6265.
65 H. Li, M. Long, H. Su, L. Tan, X. Shi, Y. Du, Y. Luo and H. Deng, *Carbohydr. Polym.*, 2022, **290**, 119482.
66 M. Jakusch, M. Janotta, B. Mizaikoff, K. Mosbach and K. Haupt, *Anal. Chem.*, 1999, **71**, 4786–4791.
67 A. M. Shrivastav, D. S. Gunawardena, Z. Liu and H.-Y. Tam, *Sci. Rep.*, 2020, **10**, 6002.